

# Candidate Tidal Dwarf Galaxies in Arp 305: Lessons on Dwarf Detachment and Globular Cluster Formation

Mark Hancock<sup>1,3</sup>, Beverly J. Smith<sup>1</sup>, Curtis Struck<sup>2</sup>, Mark L. Giroux<sup>1</sup>, & Sabrina Hurlock<sup>1</sup>  
 mhancock@ucr.edu, smithbj@etsu.edu, curt@iastate.edu, girouxm@etsu.edu, &  
 zshh7@goldmail.etsu.edu

## ABSTRACT

To search for Tidal Dwarf Galaxies (TDGs) and to study star formation in tidal features, we are conducting a large UV imaging survey of interacting galaxies selected from the Arp (1996) Atlas using the GALEX telescope. As part of that study, we present a GALEX UV and SDSS and SARA optical study of the gas-rich interacting galaxy pair Arp 305 (NGC 4016/7). The GALEX UV data reveal much extended diffuse UV emission and star formation outside the disks. This includes a luminous star forming region between the two galaxies, and a number of such regions in tidal tails. We have identified 45 young star forming clumps in Arp 305, including several TDG candidates. By comparing the UV and optical colors to population synthesis models, we determined that the clumps are very young, with several having ages  $\sim 6$  Myr. We do not find many intermediate age clumps in spite of the fact that the last closest encounter was about 300 Myr ago. We have used a smooth particle hydrodynamics code to model the interaction and determine the fate of the star clusters and candidate TDGs.

*Subject headings:* galaxies: interacting — galaxies: tidal dwarfs — galaxies: individual (Arp 305) — galaxies: numerical models

## 1. INTRODUCTION

The so-called ‘Tidal Dwarf Galaxies’ (TDG), concentrations of interstellar gas and stars in the tidal features of interacting galaxies that may become independent dwarf galaxies, have been the subject of intense scrutiny (e.g., Bournaud & Duc 2006; Recchi et al. 2006; Duc, Bournaud, & Boquien 2006). There is much uncertainty, at present, about how these structures compare with other dwarfs, in terms of their interstellar matter, their stellar populations, their dark matter content, and their star formation properties. Furthermore, the existence of such tidal dwarf galaxies has been controversial, in part because of questions about

whether they will eventually become independent galaxies. The ‘missing link’ that will unambiguously prove the tidal dwarf hypothesis is the discovery of independent dwarf galaxies that are detached from other galaxies, but have clear tidal histories.

As part of a search for TDGs and to study star formation in tidal features, we have used the Galaxy Evolution Explorer (GALEX) telescope (Martin et al. 2005) to conduct a large UV imaging survey of interacting galaxies selected from the Arp (1996) Atlas (Giroux et al. 2009). Tidal features are often very bright in the UV compared to the optical (Neff et al. 2005; Hancock et al. 2007). We have found a number of previously unstudied candidate TDGs in our sample (Giroux et al. 2009).

In this paper we investigate the interacting galaxy pair Arp 305 (NGC 4016/7). We have obtained UV and optical images of Arp 305 from the GALEX, Sloan Digitized Sky Survey (SDSS),

<sup>1</sup>Department of Physics and Astronomy, East Tennessee State University, Box 70652, Johnson City, TN 37614

<sup>2</sup>Department of Physics and Astronomy, Iowa State University, Ames IA 50011

<sup>3</sup>Now at the Institute of Geophysics and Planetary Physics, University of California, Riverside, Riverside, CA 92521

and the Southeastern Association for Research in Astronomy (SARA) telescopes. The UV images reveal extreme amounts of star formation in many different and well separated environments.

The present paper is organized as follows. In §2 we describe the observations, data reductions, morphology, and photometry, in §3 we describe our age and reddening estimates, and discuss the TDG candidates. We present a numerical model of the interaction in §4, and finally, we summarize in §5.

## 2. OBSERVATIONS

### 2.1. Observations and Reductions

Arp 305 was imaged with GALEX in both the far-UV (FUV) and near-UV (NUV) bands covering the wavelength ranges 1350Å to 1750Å and 1750Å to 2800Å, respectively. The total integration times in the FUV and NUV filters were 1584 seconds. The GALEX images have a 1.2 degree diameter, 5'' resolution and a pixel size of 1''.5. The GALEX images were reduced and calibrated through the GALEX pipeline.

The optical images were obtained as part of the SDSS (Abazajian et al. 2003) and with the SARA telescope<sup>1</sup>. The SDSS images were observed with the *ugriz* optical filters with effective wavelengths 3560Å, 4680Å, 6180Å, 7500Å, and 8870Å respectively. These SDSS images have pixel sizes of 0''.40 and the FWHM point-spread function is ~1''.2.

Arp 305 was also observed with the SARA 0.9m optical telescope on 2007 February 16, under clear skies. We used an Axiom/Apogee 2048x2048 CCD with binning set to 2 × 2 resulting in a pixel size of ~1''.2 pixel<sup>-1</sup>. A total of four 600 second exposures were made with a broadband R filter along with five 600 second images in a redshifted H $\alpha$  filter centered at 6640Å with a FWHM of 70Å. The SARA data was reduced in the standard way using the Image and Reduction Analysis Facility (IRAF<sup>2</sup>) software. We used the scaled R band image for continuum subtraction. The white dwarf Feige 34 was also observed for calibration.

<sup>1</sup><http://astro.fit.edu/sara/sara.html>

<sup>2</sup>IRAF is distributed by the National Optical Astronomy Observatories, which are operated by the Association of Universities for Research in Astronomy, Inc., under cooperative agreement with the National Science Foundation.

### 2.2. Morphology and General Properties

Arp 305 is a very wide pair with the primary galaxy, NGC 4017, to the South and the companion, NGC 4016, to the North (Figure 1). Using velocities from the NASA Extragalactic Database (NED), and assuming a Hubble constant of 75 km s<sup>-1</sup> Mpc<sup>-1</sup>, we find Arp 305 is at a distance of ~ 50 Mpc. NGC 4017 is designated as SABbc (NED) and has been classed as an ‘H II region nucleus’ galaxy by Dahari (1985). It appears nearly face-on, with two tidal tails, one pointing northwest and one to the southeast. The UV images show much extended emission to the northwest and southeast far outside the main disk. The primary seems to have an ocular waveform, a bright oval of star formation shaped like an eyelid (see Figure 2). This type of ocular structure has been observed in other galaxies, e.g., Arp 82 (Kaufman et al. 1997; Hancock et al. 2007) and IC 2163 and NGC 2207 (Elmegreen et al. 2006), and modeling has shown that it is the result of large-scale gaseous shocks from a grazing prograde encounter.

The Northern galaxy in Arp 305, NGC 4016, is designated SBdm (NED) and shows a misshapen bulge with a dusty disk. In the inner disk, a curious figure-eight shape is seen (see Figure 2). There does not seem to be any evidence to suggest that this figure-eight is an accretion feature or a wind flow. It seems too symmetric in both the GALEX and SDSS images to result from either. We suspect that the figure-eight formation in NGC 4016 is the result of a bar (see the third frame of Figure 3 in Romero-Gómez et al. 2008). More work is needed before we can fully understand the dynamic environments and formation of figure-eight features in induced bars. If the figure-eight is due to the bar, then its symmetry suggests that the inclination of the companion, like that of the primary, is low. This agrees with the presence of long tidal arms.

We find much extended UV emission in these galaxies, particularly outside the primary disk (Figures 1 and 2). Recent GALEX observations have shown a correlation between FUV emission and HI column density within the tidal tails of galaxy mergers (e.g. Neff et al. 2005; Thilker et al. 2005; Gil de Paz et al. 2005). Comparison of the UV images with the HI images

of van Moorsel (1983) shows that the UV extends out to the third HI contour ( $4.1 \times 10^{20}$ ) implying a star formation threshold of  $N_{HI} \sim 4 \times 10^{20}$  atoms  $\text{cm}^{-2}$ . For comparison, Maybath et al. (2007) found that the super star cluster (SSC) density of eight tidal regions in four merging galaxies was the highest when the HI column density was  $N_{HI} \gtrsim 4 \times 10^{20}$  atoms  $\text{cm}^{-2}$ . They also showed that this threshold is a necessary but not sufficient condition for cluster formation.

The two disks in Arp 305 are separated by  $\sim 356''$  ( $\sim 86$  kpc). Assuming an interaction velocity of  $300 \text{ km s}^{-1}$ , the two galaxies passed close by each other about 300 Myr ago. This is consistent with our numerical modeling (see §4.2). The star formation in the clumps has occurred much more recently than this (see §3.1 below).

Elmegreen, Kaufman, & Thomasson (1993) noted that this galaxy pair showed scattered debris resembling dwarf galaxies. The most prominent debris is seen in a partial residual bridge between the two spiral galaxies. This feature is particularly striking in the GALEX images (Figure 1). For simplicity, we will adopt the name ‘bridge TDG’ for the tidal dwarf candidate in the residual bridge. With SARA, we have detected H $\alpha$  emission from this feature confirming that it is at the same redshift as the galaxies (Figure 2). This structure is clearly detected in HI (van Moorsel 1983), further suggesting that it is part of the Arp 305 system. HI emission can be seen extending from the main NGC 4017 disk North toward the companion.

NGC 4016 and NGC 4017 have total masses of  $1.7$  and  $16.2 \times 10^{10} M_{\odot}$  and HI masses of  $2.1$  and  $7.1 \times 10^9 M_{\odot}$ , measured out to  $\sim 1'.5$  and  $\sim 3'.5$  respectively (van Moorsel 1983). In an HI survey of Arp galaxies, Bushouse (1987) give a median HI mass for their sample of  $1.8 \times 10^9 M_{\odot}$ .

Using the calibration in Jester et al. (2005) we converted the total g band luminosity of the two galaxy disks to a total Johnson B luminosity. NGC 4016 and NGC 4017 have L(B) of  $\sim 4 \times 10^9 L_{\odot}$  and  $\sim 9 \times 10^9 L_{\odot}$  respectively. For comparison, the median L(B) in the Bushouse (1987) Arp sample is  $2.6 \times 10^{10} L_{\odot}$ . NGC 4016 and NGC 4017 are fainter in B than 97% and 16% respectively, of the Bushouse (1987) sample of interacting disk-type galaxies, thus NGC 4016 is somewhat low luminosity. NGC 4016 and NGC

4017 have mass/luminosity ratios,  $M_{HI}/L(B)$ , of 0.5 and 0.8 respectively. The  $M_{HI}/L(B)$  of NGC 4016/7 are greater than 77% and 92% of the Bushouse (1987) sample respectively. Thus Arp 305 is a relatively gas rich system.

Our SARA data indicate that NGC 4016/7 have H $\alpha$  luminosities of  $6.4 \times 10^{40}$  and  $1.9 \times 10^{41}$  erg  $\text{s}^{-1}$  respectively. These are similar to the median H-alpha luminosities of the Bushouse (1987) studies  $4.6 \times 10^{40}$  erg  $\text{s}^{-1}$ .

### 2.3. Photometry

We have identified 45 star forming clumps in Arp 305 in the GALEX FUV images (Figure 2). The bridge TDG contains four of these clumps (labeled clumps 12, 13, 15, and 16 in Figure 2). Two additional possible detached TDG candidates northeast and southwest of NGC 4016 are marked in Figure 2 (clumps 1 and 19).

We performed aperture photometry on these clumps with the IRAF task PHOT. For the clumps, we used circular apertures of radii  $5''$  in all bands. This corresponds to 3.3 and 12.6 pixels in the GALEX and SDSS images respectively. For background subtraction of the GALEX and SDSS data we adopted a 5 pixel wide annulus with radii of 4 and 14 pixels respectively. For the entire bridge TDG, NGC 4016 disk, and NGC 4017 disk we used circular apertures of radii  $37''.5$ ,  $60''$ , and  $82''.5$  respectively in all bands. The clumps in the disks and some of the tidal regions are often crowded. Additionally, the backgrounds in the disks change rapidly. The sky values for our photometry were determined from the median of the sky pixels, which is useful for computing sky values in regions with rapidly varying sky backgrounds. We made a second sky determination using the mode of the same the same sky annuli which is suited for measuring stellar objects in crowded fields. The difference in the two resulting magnitudes was added as an additional source of uncertainty to our measurements.

Because there were no suitable stars in the Arp 305 FUV field we adopted the aperture corrections used for photometry of clumps in Arp 82 of 1.15 for the FUV and 1.45 for the NUV (Hancock et al. 2007). The UV fluxes were converted to magnitudes on the AB system (Oke 1990).

For the SDSS optical data, the aperture correc-

tions were determined by measuring three stars in the field. The flux aperture corrections for the *ugriz* SDSS data are 1.08, 1.04, 1.07, 1.12, and 1.03 respectively.

Table 1 lists the total magnitudes for the bridge TDG and the two disks, where the first column is the object, the second through eighth columns are the FUV, NUV, u, g, r, i, and z magnitudes respectively. The clump magnitudes are listed in Tables 2, 3, and 4. In each table, the first column is the clump number, the second column describes the clump (e.g. a tidal feature or a disk clump), the third through ninth columns are the FUV, NUV, u, g, r, i, and z magnitudes respectively.

### 3. RESULTS

#### 3.1. Reddening and Ages

Several of the star forming clumps in Arp 305, including the four in the bridge TDG, are very blue suggesting very recent star formation. To estimate the ages of the star forming clumps we have generated a set of model cluster spectral energy distributions (SED) using the stellar population synthesis code Starburst99 (SB99) (Leitherer et al. 1999). We used the v5.1 code with the Padova tracks which include the asymptotic giant branch (AGB) stellar models (Vázquez & Leitherer 2005). The SB99 models were generated assuming stellar and nebular continuum emission, a single burst population, solar metallicity, a Kroupa IMF (Kroupa 2002) from 0.1 to  $100 M_{\odot}$ , and a total mass of  $10^6 M_{\odot}$ . The model ages range from 1 Myr to 10 Gyr. To compare with the observations, the models were reddened from 0–2.0 mag in 0.02 mag increments assuming the Calzetti, Kinney, & Storchi-Bergmann (1994) starburst reddening law. We have included H $\alpha$  line emission in our model SEDs, as it can have a significant effect on the colors of young clusters (e.g. Smith et al. 2008). Finally, the SEDs were convolved with the GALEX and SDSS bandpasses. Once the model IMF and metal abundance is defined, the location of the clumps on a color-color diagram depend only on the age and reddening.

Figure 3 plots the FUV-NUV color against the NUV-g color. The solid black squares are clumps in the bridge TDG (clumps 12, 13, 15, and 16), the open blue squares are clumps in NGC 4016, the solid blue triangles are clumps 1 and 19, and

a green x represents clumps in NGC 4017. The curves are SB99 models with E(B–V) from 0 to 0.5 mags. The model ages increase up and to the right (on this figure) from 1 Myr to 10 Gyr. The other color-color figures are similar so are not shown.

To estimate the ages and reddenings of the clumps, we compared the available measured colors to each of the reddened SB99 model colors. We used a  $\chi^2$  calculation to determine the fit of the observed colors to that of the models and hence the ages of the clumps. The ages and extinctions associated with the minimum  $\chi^2$  are taken as the best-fit values (Hancock et al. 2008). To determine the uncertainties in the predicted ages we find the minimum and maximum ages within a  $\Delta\chi^2$  defined to give a 68% confidence level (e.g., Press et al. 1992). Additionally, the model step sizes were added to the age and E(B–V) uncertainties (see Hancock et al. 2008; Smith et al. 2008 for more details on estimating ages and age uncertainties). We note that, because some of the clump’s masses are possibly low, stochastic sampling of the IMF could affect the age determinations (e.g., Cerviño & Valls-Gabaud 2003). We do not include this effect in our calculations.

The ages are listed in Table 5 where the first column is the clump number, the second column is the clump ID, the third and fourth columns are the R.A. and Dec., the fifth column is the age estimate, the sixth column is the estimated E(B–V), and the seventh column lists the colors used to determine the ages. Note that we did not include upper limits in our fits.

From Table 5 we find the mean best-fit age of the clumps in the bridge TDG is  $19_{-15}^{+36}$  Myr. The two other TDG candidates, clump 1 and clump 19, have best-fit ages of  $236_{-26}^{+23}$  and  $7_{-2}^{+43}$  Myr respectively. Given the precision of our age estimates, the results in Table 5 suggest that, with the exception of clump 1, the most recent star formation occurred in all the clumps at about the same time,  $\lesssim 10$  Myr ago.

We do not find many intermediate age clumps in spite of the fact that the last closest encounter was about 300 Myr ago (see §2.2 and §4). One possible explanation is a selection effect. We selected the clumps from the FUV image so have chosen the youngest clumps. Another possibility is our limited resolution. By definition the clumps

are  $5''$  or 1.2 kpc in radius (see §2.3). It is likely that the clumps are made up of several unresolved clusters and/or associations. The light would be dominated by the younger clusters.

It seems likely that our clumps are clusters of clusters that fill a significant part of our resolution element. After 300 Myr some of the clusters may have dissolved. More importantly, if a cluster of clusters (a clump) is not bound, the individual clusters may have simply separated, so that a resolution element centered on any one of them would not include the others. Intermediate age clusters are likely too faint for our observations. The absence of intermediate age clumps in the tidal structures of Arp 305 and some other systems (e.g. Arp 82 and Arp 285; Hancock et al. 2007; Smith et al. 2008) indicates that it is hard to make long-lived TDGs.

We note that the FUV–NUV colors of several clumps (mostly in the southeast tidal region of NGC 4017) do not match our SB99 models within the  $1\sigma$  uncertainties, in that they are too blue (Figure 3), however, they are consistent within  $2\sigma$ . These clumps might be foreground stars or distant quasars, however, they do appear within the extended diffuse UV emission. Alternatively, our adopted uncertainties might be too small since we have not included uncertainties associated with the aperture corrections. A third possibility is that the solar metallicity we have assumed may be too high for our tidal features. The GALEX FUV–NUV color is bluer for lower metallicity (e.g. Boissier et al. 2008).

### 3.2. The Bridge TDG

The bridge TDG looks to be embedded in a massive HI plume stretching North from the primary (van Moorsel 1983). Four clumps in the bridge TDG (clumps 12, 13, 15, and 16) are visible in the GALEX image, but only two (clumps 12 and 13) are prominent in the H $\alpha$  and SDSS images. This suggests that the latter two are younger, have more O-stars, or less extinction. Our age and extinction estimates of these clumps are not precise enough to show such a difference (Table 5).

The star formation in the bridge TDG most likely started after it was separated from the host disks. The distance between the nucleus of the primary and clump 13 in the bridge TDG is  $2.5$ ,

$\sim 36$  kpc. The clumps in the bridge TDG are an average of 19 Myr old. To travel 36 kpc in 19 Myr the material would have to travel at a velocity of roughly  $2000 \text{ km s}^{-1}$  relative to the primary. The HI kinematics do not support this (van Moorsel 1983).

Based on our best-fit models and scaling to the SDSS r flux, we estimate that the stellar masses for clumps 12, 13, 15, and 16 in the bridge TDG are  $0.3 - 2.7 \times 10^6 M_\odot$ ,  $0.3 - 2.1 \times 10^6 M_\odot$ ,  $0.1 - 0.9 \times 10^6 M_\odot$ , and  $0.1 - 1.6 \times 10^6 M_\odot$  respectively, giving a total stellar mass for the bridge TDG of  $\sim 1 - 7 \times 10^6 M_\odot$ . These clump masses are consistent with that of Galactic globular clusters (e.g., Pryor & Meylan 1993) and Super Star Clusters (SSC) (e.g. Holtzman et al. 1992, 1996; O’Connell, Gallagher, & Hunter 1994; Schweizer et al. 1996; Whitmore et al. 1993; Whitmore & Schweizer 1995; Watson et al. 1996). For comparison, the TDG candidates in Higdon, Higdon & Marshall (2006) have masses around  $2 \times 10^7 M_\odot$  to  $3 \times 10^8 M_\odot$ .

The HI mass of the bridge TDG, as estimated from the contours in van Moorsel (1983), is  $\sim 6 \times 10^7 M_\odot$ . consistent with the 29 low mass dwarfs studied in Begum et al. (2008) ( $10.18 - 81.14 \times 10^6 M_\odot$ ). This means that the HI mass of the bridge TDG is about a factor of 9 to 60 greater than the stellar mass.

From the SDSS magnitudes, we estimate a total blue luminosity for the bridge TDG of  $6.1 \times 10^7 L_\odot$ , in the range of the irregular and blue compact dwarfs studied by Hunter & Elmegreen (2004). The HI mass/luminosity ratio for the bridge TDG is  $M_{HI}/L(B) \sim 1 M_\odot/L_\odot$ , similar to those of irregular and compact blue dwarfs (e.g. Hunter & Elmegreen 2004; Pisano et al. 2005; Tarchi et al. 2005; Begum et al. 2008). The bridge TDG has an H $\alpha$  luminosity of  $3.2 \times 10^{39} \text{ erg s}^{-1}$ , similar to the H $\alpha$  luminosities of the dwarfs in Hunter & Elmegreen (2004) and the tidal features studied by Smith & Struck (2001).

The bridge TDG is considerably more luminous than the star forming regions seen in the HI bridge in the M81/M82 complex (Arp’s Loop) (e.g. de Mello et al. 2008; Boyce et al. 2001; Sun et al. 2005). However, they do have similar HI column densities. The M81/M82 bridge has  $n(\text{HI}) \sim 5 - 30 \times 10^{20} \text{ atoms cm}^{-2}$  (de Mello et al. 2008), while the Arp 305 bridge TDG has  $n(\text{HI}) \sim 4 \times 10^{20} \text{ atoms cm}^{-2}$ . For comparison, the HI

bridge between the Magellanic clouds has typical HI column densities  $\sim 10^{20} - 10^{21}$  atoms  $\text{cm}^{-2}$  (Muller et al. 2003, 2004).

### 3.3. Other Clumps of Interest

To the southwest of NGC 4016 is a bright clump, number 1, that appears to be at the tip of a faint tidal arm. This clump is bright in both the GALEX UV and all the SDSS optical bands and is within the extended HI envelope (van Moorsel 1983). It is not detected in our continuum subtracted H $\alpha$  images and has an H $\alpha$  luminosity  $3\sigma$  upper limit of  $1.4 \times 10^{39}$  erg  $\text{s}^{-1}$ . Clump 1 is the oldest clump in our sample (Table 5). We can not rule out the possibility that this object is a foreground star or a background object.

To the northeast is another possible TDG, clump 19. The northern tail of NGC 4016 points toward this clump. Clump 19 is also bright in both the GALEX UV and all the SDSS optical bands, and is not detected in our continuum subtracted H $\alpha$  images with an  $3\sigma$  H $\alpha$  upper limit of  $2.2 \times 10^{39}$  erg  $\text{s}^{-1}$ . Unfortunately, the HI figure in van Moorsel (1983) does not cover the region of the sky that includes clump 19. Figure 2 shows clump 19 to be an extended object with an appearance similar to an inclined disk. Given this, the lack of an H $\alpha$  detection, and the large distance from NGC 4016 ( $\sim 70$  kpc), we can not rule out the possibility that clump 19 is a background galaxy.

In the northwest tail of the southern galaxy, NGC 4017, there is another potential TDG, clump 11 (Figure 2). This clump is seen clearly in the UV, optical, and H $\alpha$  maps. It has an H $\alpha$  luminosity of  $2.4 \times 10^{39}$  erg  $\text{s}^{-1}$ .

Using the same technique described above we find that clump 1 and clump 19 have stellar masses of  $\sim 1.9 - 2.1 \times 10^7 M_{\odot}$  and  $\sim 0.6 - 5 \times 10^7 M_{\odot}$  respectively. These masses are consistent with those of TDGs and more massive than Galactic globular clusters. Clump 11 has a mass of  $0.45 - 3.8 \times 10^6 M_{\odot}$ , similar to globular clusters and SSCs.

Near the bases of both the northeastern and southwestern tidal tails in NGC 4017 are extremely luminous clumps (clumps 22 and 32). These ‘hinge clumps’ likely form when material is pulled out from deeper in the original disk.

This material, gas with higher initial densities, is more compressed. Moreover, being pulled out in a tail likely reduces the shear levels of the original disk, allowing self-gravity to more easily form big clouds. The ‘hinge clumps’ are the two brightest UV clumps in the primary and are very bright in H $\alpha$ . Clumps 22 and 32 have H $\alpha$  luminosities of  $1.1 \times 10^{40}$  erg  $\text{s}^{-1}$  and  $1.2 \times 10^{40}$  erg  $\text{s}^{-1}$  respectively and account for about 6% of the total H $\alpha$  flux of NGC 4017. A luminous ‘hinge clump’ was also observed in Arp 82 at the base of the long extended northern tail (Hancock et al. 2007).

## 4. NUMERICAL HYDRODYNAMICAL MODEL OF THE ENCOUNTER

### 4.1. Morphological Constraints

The long tidal tails and bridges in this system, and the nearly comparable sizes of the visible galaxies, immediately suggest the action of strong tidal forces. The ocular morphology of the NGC 4017 disk, and the possibly collisionally induced bar-like morphology of the NGC 4016 disk reinforce this impression. All of these characteristics are indicative of a prograde fly-by encounter (see Struck 1999). The fact that the disturbances are comparable for both galaxies suggests that the interaction was prograde for both and that they are of comparable mass. The somewhat more disordered appearance of NGC 4016 may suggest a slightly lower mass, and perhaps a greater disk inclination relative to the orbital plane.

These are the primary observational clues the system provides to constrain models. Secondary constraints include the detailed wave structure within the disks. Another secondary constraint is the large separation of the galaxies, which together with the very small velocity difference of the two galaxies (van Moorsel 1983) suggests that they are bound and near their point of greatest separation.

Because the tidal disturbance is so strong, we suspect that the point of closest approach was very close. Yet, because of the lack of ring-like structures we doubt that the disks inter-penetrated to a large degree. Thus, with a good idea of the geometry of the collision, of closest and farthest separations, of galaxy masses and the current kinematic interaction age, a dynamical model is quite well constrained.

## 4.2. Model Details

Both the smooth particle hydrodynamical (SPH) simulation code and the collision parameters used to produce the model described below are very similar to those used in our recent study of the Arp 285 system (Smith et al. 2008). More details on the code are also provided in Struck (1997). We will summarize the defining parameters of the present model, but not repeat all of the details provided in those earlier works.

The two model galaxies have rigid, dark halo potentials. These potentials have a softened power-law form, such that their rotation curves rise linearly in a core region and decline very slowly at large radii (as  $r^{-0.1}$ ). Both halos have the same form (Eq. (1) of Smith et al. 2008) and the same softening length of 3 kpc in the adopted scaling. The ratio of the companion to primary halo mass is 0.8.

A total of 42,900 particles were used to model the gas disk of the primary (corresponding to NGC 4017), and 18,090 were used for the companion (NGC 4016) gas disk. Small old star disks were also included in the model, but will not be discussed here. The model unit of length was 1.0 kpc, and the time unit was 200 Myr (as in Smith et al. 2008). With these units the initial radii of the gas disks were 10.8 kpc for the primary and 6.0 kpc for the companion. The latter seems somewhat small, but is still sufficient to yield an enormous tidal tail after the encounter (see Figure 4). The halo scale mass of the primary (see definition in Smith et al. 2008) is  $M_h = 1.5 \times 10^{10} M_\odot$ .

The primary disk was initialized in the x-y plane. The companion disk is first set up in the x-y plane, then rotated  $30^\circ$  around a y-axis through its center, and then  $90^\circ$  around the z-axis passing through its center. The relative orbit of the companion is in the x-y plane, so from the point of view of the companion disk, the primary approaches at a moderately steep angle. The relative orbit of the companion is in the same sense as the rotation of the primary, so it sees the encounter as prograde. Before it is tilted, the companion disk orbits in the same (counter-clockwise) sense, so it also sees the encounter as prograde. (This is the most significant difference from the Arp 285 model of Smith et al. 2008).

The initial position of the companion relative

to the primary center is (-8.92, -20., 0.0) kpc. Its initial relative velocity is (240, 75, 0.0) km  $s^{-1}$ . The model includes the effects of a Chandrasekhar type dynamical friction, as described in Struck & Smith (2003).

Simple optically thin radiative cooling is included, as is feedback heating from star-forming regions, as described in Struck (1997). In the model a particle turns on star formation when it is cool (e.g., below about 8000 K) and exceeds a threshold density value. A constant threshold value is used throughout the model. However, it is our experience that the results do not depend greatly on the precise value of this threshold. This is because when the threshold is exceeded, the local self-gravity included in the model dominates, so any reasonable threshold value will be exceeded, until the heating is initiated.

## 4.3. Model Results

We should note that our philosophy was to produce an approximate model as an aid to interpreting the observations, so we have not run an extensive grid of models in order to produce a very precise representation of the system. Nonetheless, the model results do provide helpful input for interpreting this system and projecting its future.

Figure 4 and Figure 5 show that the model orbit is quite elliptical (non-circular), which is required by the constraints discussed in §4.1. The four snapshots of Figure 4 show the overall evolution of the system from a time just after closest approach, in the first panel, to the onset of merger in the final panel. The two intermediate times shown in the second and third panels bracket the present, indicating that about 300 – 400 Myr has passed since the point of closest approach. Because the disk of the primary is in the plane of the relative orbit, it is strongly affected by the encounter, and produces a strong bridge and counter-tail, shown by red dots in Figure 4. This is in general agreement with the HI observations. The model suggests that essentially all of the bridge material originates in the primary.

Despite its tilt relative to the orbital plane, the companion (corresponding to NGC 4016), produces a strong counter-tail (shown by green dots). It produces only a very short bridge component. These features are in general, but not

complete, agreement with observation. The position of clump 1 suggests a longer southern extension. On the other hand, the HI data show no long gas plume to the South. The HI map does show a feature to the northeast of NGC 4016, and clump 19 is also found in that area. These features support the existence of a strong counter-tail. However, the model tail is in the northwest, not the northeast. If the second and third panels of the Figure 4 were rotated by about  $30^\circ$  then the positions of the galaxies would agree better with the observations, and the tail would lie more to the North. Nonetheless, somewhat different values of the collision parameters or companion potential parameters would be needed to put the tail in the northeast.

The last three panels of Figure 4 illustrate the star formation (SF) characteristics of the model. First of all it is clear that SF is maintained in the centers of both galaxies for the duration of the encounter. (This is confirmed by snapshots at other times.) This is not surprising since prograde flybys subtract orbital angular momentum from material in parts of the affected disk, just as they add it to the sectors that generate bridges and tails. This leads to an extended period of central compression as this material moves inward.

Our data suggest that clumps with ages greater than 20 Myr are rare in Arp 305. The model shows SF in all the tidal features from the time of their formation to the present. However, the (model) SF rate is low in the bridge. The small number of clusters observed there and their age distribution are in qualitative accord with that result. Interestingly, in the model SF occurs in the middle of the bridge and at the bridge base near the primary, but there is gap in between and towards the companion, as in the observations. This is seen over a range of times, but the small numbers of SF particles in the model preclude firm conclusions. Material balanced between the two galaxies in the middle of the bridge may be better able to pull together than that in the radially sheared parts of the bridge that are falling onto one of the galaxies.

Also in accord with the observations, SF is relatively strong in the primary counter-tail (Southern tail of NGC 4017) and weak in that of the companion (region northeast of NGC 4016). The latter is tidally sheared to a much greater length than the former; the South primary tail stays much closer

to its parent disk. Thus, we expect the gas surface density to be greater in the Southern tail.

Finally, the model does not account for SF to the northwest of the primary disk, in the vicinity of clumps 11, 14, and 42 in the observations. We speculate that this is material splashed out of the disks at closest approach. If the distance of closest approach was only a little smaller, the model would have more of this ‘splash’ material.

Nonetheless, the model does a good job in accounting for the overall SF characteristics of the system. We again emphasize how similar this system is to the Arp 285 system. The modeling suggests that the primary difference is that the encounter was not as strong (nor ‘prograde’) for the companion in Arp 285, but the mass transfer from the primary was greater.

#### 4.4. Future Projections: The Fate of the Clusters and Dwarfs

##### 4.4.1. Mid-term Futures: Building a Globular Cluster System

Star-forming particles or groups of particles in the model represent new star clusters or TDGs. Previous studies (e.g., of M51, Bastian 2005 and the Antennae, Fall, Chandar, & Whitmore 2005) suggest that many of these will soon disappear as a result of unbinding due to gas expulsion and other forms of ‘infant mortality.’ These processes cannot be resolved in the present models.

Related questions include: what is the long term fate of the clusters that do survive, and do any of those that might represent tidal dwarfs detach in some sense? We have investigated those questions by running our models beyond the present, up to the time of merger, and followed the trajectories of specific star-forming particles as shown in Figure 5. We note that the tracked particles remained gas particles in the model, and thus, subject to the effects of shocks, in contrast to real star clusters. This is generally a small problem, since in most cases the trajectories of these particles are ballistic in the changing potential of the two galaxies, and hydrodynamic effects like the collision of two gas streams is rare before merger.

The upper two panels of Figure 5 illustrate the fate of SF particles in the bridge. The upper left panel shows the trajectories of particles that



turned on SF as the bridge was forming. Although they are formed in a small region, their trajectories bifurcate. Some fall promptly into the primary, others are captured by and orbit the companion. (The zig-zag trajectories of the latter represent orbits around the companion.)

The particle in the upper right panel turned on SF at a time and place like that of the bridge TDG in the observations, and might illustrate the fate of the bridge TDG. If so, that fate is to be promptly captured by the companion and carried into the merger. It seems very unlikely that TDGs formed in the bridge will detach and survive the merger.

The lower left panel shows clusters formed in the companion counter-tail. The story here is similar to that of the bridge in that there is a bifurcation between particles that remain bound to the companion and those that ‘escape’ to a region dominated by the combined potential. These latter include particles in the outer tail with significant radial velocities relative to the center of mass at the time of SF. A comparison to the last panel of Figure 4 shows that they are among the particles scattered around the residual tail after merger. Although they are bound to the joint potential, these particles are detached in the sense that they are not contained within the sphere of influence of either individual galaxy before merger. These trajectories suggest that clump 19 may be similarly detached.

We note that our model results in very few particles near the location of clump 1. The few that are found there remain tightly bound to the companion, with no hope of becoming detached.

The last panel of Figure 5 shows the fate of clusters formed in the primary counter-tail. Essentially all are retained by the primary, though the orbit of at least one is strongly influenced by the companion. Nonetheless, the orbits of some of these make excursions out to radii of tens of kpc. Clumps 36–40 and 43–45 may follow similar orbits and may be future members of the globular cluster or dwarf satellite system of the merger remnant. It is possible that this tidal tail, along with the bridge and the inner part of the companion tail, is the nursery of an incipient globular cluster system. This scenario is supported by the recent results of Bournaud, Duc, & Emsellem (2008).

#### 4.4.2. Long-term Future of the Far-Flung Tidal Dwarf Candidates

The TDG candidates born in the outer tail have very low angular momentum relative to the merger remnant, so we expect that they have very radial orbits. Figure 6 shows the results of an attempt to learn about their long-term future. This figure shows the gas particle distribution at the time of the last panel in Figure 4, when the merging process is well advanced. The plus signs show the location of two of the TDG candidates from the lower left panel of Figure 5. Their association with the tail is clear. The two curves show projections of their trajectories a couple Gyr into the future. These trajectories are analytic approximations. Specifically, particle positions at late times were output from the numerical model and used to fit a p-ellipse curve from Struck (2006). These curves have been shown to give quite accurate representations of orbits in fixed power-law potentials (Struck 2006; Lynden-Bell & Jin 2008). We assume that the potential fluctuations in the final stages of merging are small, so that the global potential is well approximated as the sum of the two individual halo potentials. Both potentials have the same form, which is a power-law outside a small core radius.

The analytic curves show us that the TDG candidates fall into the merger remnant with other tail material. For the two particles shown the radii of closest approach are 5.3 and 7.4 kpc. Although these are only estimates, they suggest that the objects will come close enough to experience substantial tidal disruption. This is even more likely since they have negligible dark matter halos to help hold them together. The curves shown in Figure 6 do not include the effects of dynamical friction, which are likely to be considerable given the close approach. Overall we expect these dwarf candidates to be disrupted or reduced to a small core and left on a smaller orbit after the first close passage.

In their extensive N-body study of tidal dwarf formation Bournaud & Duc (2006) found that 75% of the dwarf candidates fell back into the galaxies within a few  $\times 10^8$  yr. The remaining 25% had a typical lifetime of more than 2 Gyr. Most of the later formed in the outer parts of tidal tails. The outer tail objects in the lower left panel of Figure 5 are the same kind of relatively

long-term survivors. Even though their existence may consist of a single excursion into the outer halo before fall and destruction, that process can take several Gyr. We suspect very few live much longer.

Globular clusters on the other hand, can survive close passages of more than several kpc. Both observations and models suggest that cluster formation is quite prolific in this type of interaction, and dozens could be produced in the bridge and tails.

## 5. SUMMARY

We present UV and optical images of Arp 305 (NGC 4016/7) from the GALEX, SDSS, and SARA telescopes. The primary, NGC 4017, seems to have an ocular waveform, while the Northern galaxy, NGC 4016, has an interesting figure-eight structure that may be due to a bar. We have found active star formation in various tidal features outside the main galaxy disks. A prominent TDG is seen in a partial residual bridge between the two spiral galaxies, with a total HI mass of  $6 \times 10^7 M_{\odot}$  and a mass/luminosity ratio of  $M_{HI} / L(B) \sim 1 M_{\odot}/L_{\odot}$ .

We have identified 45 young star forming clumps from the GALEX FUV image of Arp 305. By comparing the various UV and optical colors to SB99 models, we determined that the clumps are very young, with several having ages  $\sim 6$  Myr (Table 5).

We do not find many intermediate age clumps in spite of the fact that the last closest encounter was about 300 Myr ago (see §2.2 and §4). The absence of intermediate age clumps in the tidal structures of Arp 305 and some other systems (e.g. Arp 82 and Arp 285; Hancock et al. 2007; Smith et al. 2008) indicates that it is very hard to make long-lived TDGs.

The stellar masses of the four clumps in the bridge TDG are between  $\sim 10^5$  and  $\sim 3 \times 10^6 M_{\odot}$  and the total stellar mass of the bridge TDG is  $\sim 1 - 7 \times 10^6 M_{\odot}$ . Our mass estimates suggest that the bridge TDG might be a system of young globular clusters or SSCs. Clump 1 and clump 19 have implied stellar masses of  $\sim 1.9 - 2.1 \times 10^7 M_{\odot}$  and  $\sim 0.6 - 5 \times 10^7 M_{\odot}$ , if they are at the distance of Arp 305. These masses are consistent with TDGs and are larger than Galactic globular clusters.

We have used an SPH code to model the interaction and determine the fate of the candidate TDGs. The model does a good job in accounting for the overall SF characteristics of the system. Our model suggests that the fate of the bridge TDG is to be promptly captured by the companion and carried into the merger. It seems very unlikely that TDGs formed in the bridge will detach and survive the merger. Our model resulted in very few particles near the location of clump 1. The few that are found there remain tightly bound to the companion, with no hope of becoming detached. Clump 19 is the best candidate for a soon-to-detach TDG, if it is at the same redshift as Arp 305.

The present system illustrates how tidal structures can be prolific producers of the precursors of globular clusters. The eventual merger of the galaxies may lead to the production of even more, as in the well-known Antennae system. However, these are unlikely to orbit very far out into the halo, while those produced in the tails have a much better chance of forming a system of halo globulars.

We thank the GALEX and SDSS teams for making this research possible. GALEX is a NASA Small Explorer mission, developed in cooperation with the Centre National d'Etudes Spatiales of France and the Korean Ministry of Science and Technology. This research was supported by NASA LTSA grant NAG5-13079 and GALEX grant GALEXGI04-0000-0026. This work has made use of the NASA/IPAC Extragalactic Database (NED), which is operated by the Jet Propulsion Laboratory, California Institute of Technology, under contract with NASA.

## REFERENCES

- Abazajian, K, et al. 2003, AJ, 126, 2081
- Arp, H. 1966, Atlas of Peculiar Galaxies (Pasadena: Caltech)
- Bastian, N. 2005, A&A, 431, 905
- Begum, A., Chengalur, J. N., Karachentsev, I.D., & Sharina, M. E. 2008, MNRAS, 386, 138
- Boissier, S. et al. 2008, ApJ, 681, 244

- Bournaud, F., Duc, P.-A., & Emsellem, E. 2008, MNRAS, 289, 8
- Bournaud, F. & Duc, P. -A. 2006, A&A, 456, 481
- Boyce, P. J. et al. 2001, ApJ, 560, 127
- Bushouse, H. 1987, ApJ, 320, 49
- Calzetti, D., Kinney, A. L., & Storchi-Bergmann, T. 1994, ApJ, 429, 582
- Cerviño, M. & Valls-Gabaud, D. 2003, MNRAS, 338, 481
- Dahari, O. 1985, ApJS, 57, 643
- de Mello, D. F., Smith, L. J., Sabbi, E., Gallagher, J. S., Mountain, M., & Harbeck, D. R. 2008, AJ, 135, 548
- Duc, P. -A., Bournaud, F., & Boquien, M. 2006, in IAU Symp. 237, ed. B. G. Elmegreen, & J. Palous, 323
- Elmegreen, D. M., Elmegreen, B. G., Kaufman, M., Sheth, K., Struck, C., Thomasson, M., & Brinks, E. 2006, ApJ, 642, 158
- Elmegreen, B. G., Kaufman, M., & Thomasson, M. 1993, ApJ, 412, 90
- Fall, S.M., Chandar, R., & Whitmore, B. C. 2005, ApJ, 631, L133
- Gil de Paz A., et al., 2005, ApJ, 627, L29
- Giroux, M. L. et al. 2009, in preparation
- Hancock, M., Smith, B. J., Giroux, M. L., & Struck, C. 2008, MNRAS, 389, 1470
- Hancock, M., Smith, B. J., Struck, C., Giroux, M. L., Appleton, P. N., Charmandaris, V., & Reach, W. T. 2007, AJ, 133, 676
- Higdon, S. J. U., Higdon, J. L., & Marshall, J. 2006, ApJ, 640, 783
- Holtzman, J. A., et al. 1992, AJ, 103, 691
- Holtzman, J. A., et al. 1996, AJ, 112, 416
- Hunter, D. A. & Elmegreen, B. G. 2004, AJ, 128, 2170
- Jester, S. et al. 2005, AJ, 130, 873
- Kaufman, M., Brinks, E., Elmegreen, D. M., Thomasson, M., Elmegreen, B. G., Struck, C., & Klaric, M. 1997, AJ, 114, 2323
- Kroupa, P. 2002, Science, 295, 85
- Leitherer, C., et al. 1999, ApJS, 123, 3
- Lynden-Bell, D., & Jin, S. 2008, MNRAS, 386, 245
- Maybhate, A., Masiero, J., Hibbard, J. E., Charlton, J. C., Palma, C., Knierman, K. A., & English, J. 2007, MNRAS, 381, 59
- Martin, D. C., et al. 2005, ApJ, 619, L1
- Muller, E., Stanimirović, S., Rosolowsky, E., & Staveley-Smith, L. 2004, ApJ, 616, 845
- Muller, E., Staveley-Smith, L., Zealey, W., & Stanimirović, S. 2003, MNRAS, 339, 105
- Neff, S. G., et al. 2005, ApJ, 619, L91
- O'Connell, R. W., Gallagher, J. S., & Hunter, D.A. 1994, ApJ, 433, 65
- Oke, J., B., 1990, AJ, 99, 1621
- Pisano, D. J., Koo, D. C., Willmer, C. N. A., Noeske, K. G., & Phillips, A. C. 2005, ApJ, 630, L25
- Press, W. H., Teukolsky, S. A., Vetterling, W. T., & Flannery, B. P. 2002, Numerical Recipes in Fortran: the art of scientific computing, 2nd ed. (Cambridge University Press)
- Pryor, C., & Meylan, G. 1993, in ASP conf. Series, Vol. 50, Structure and Dynamics of Globular Clusters, ed. S. G. Djorgovski & G. Meylan (San Fransisco: ASP), 357
- Recchi, S., Theis, C., Kroupa, P., & Hensler, G. 2007, A&A, 470, 5
- Romero-Gómez, M., Athanassoula, J. J., & García-Gómez, C. 2008, astro-ph/0801.3412
- Schweizer, F., Miller, B. W., Whitmore, B. C., & Fall, S. M. 1996, AJ, 112, 1839
- Smith, B. J., et al. 2008, AJ, 135, 2406
- Smith, B. J. & Struck, C. 2001, AJ, 121, 710
- Struck, C. 1997, ApJS, 113, 269

- Struck, C. 1999, Phys Rep, 321, 1
- Struck, C. 2006, AJ, 131, 1347
- Struck, C., & Smith, B. J. 2003, ApJ, 589, 157
- Sun, W. -H. et al. 2005, ApJ, 630, 133
- Tarchi, A., Ott, J., Pasquali, A., Ferraras, I., Castangia, P., & Larsen, S. S. 2005, A&A, 133, 136
- Thilker D.A., et al., 2005, ApJ, 619, L79
- van Moorsel, G. A. 1983, A&AS, 54, 19
- Vázquez, G. A. & Leitherer, C. 2005, ApJ, 621, 695
- Watson, A. M., et al. 1996, AJ, 112, 534
- Whitmore, B. C. & Schweizer, F. 1995, AJ, 109, 960
- Whitmore, B. C., Schweizer, F., Leitherer, C., Borne, K., & Robert, C. 1993, AJ, 106, 1354

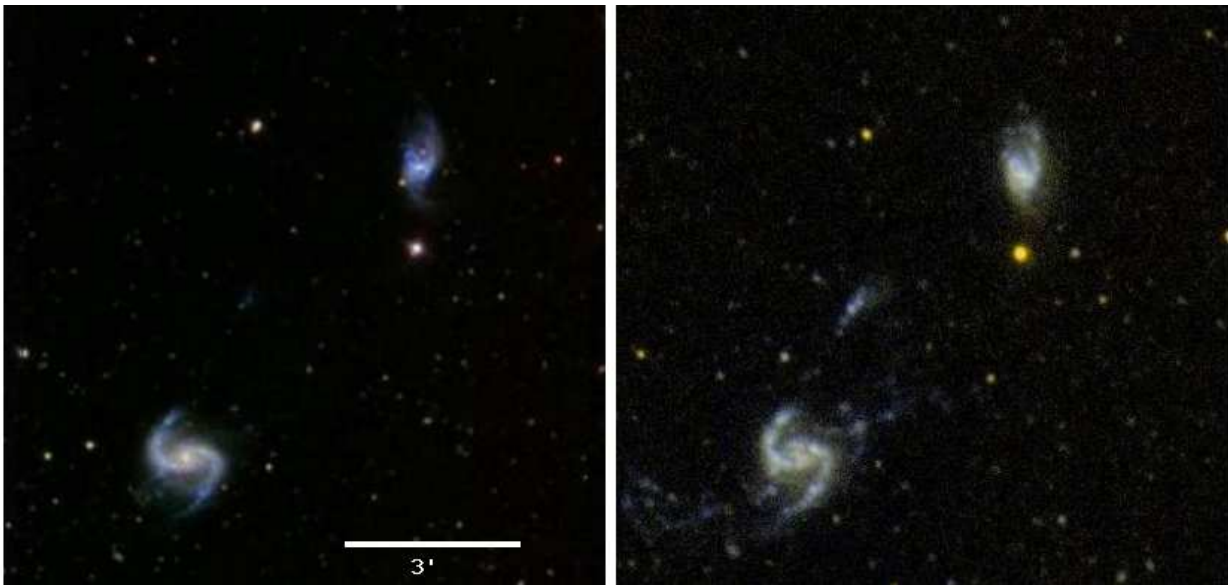


Fig. 1.— Left: Composite *ugriz* SDSS image of Arp 305. North is up and East is to the left. Right: Composite FUV (blue) and NUV (yellow) GALEX image of Arp 305. North is up and East is to the left. The northern galaxy is NGC 4016, while the southern is NGC 4017. The bridge TDG is clearly seen between the two galaxies and clump 1 is seen southwest of the NGC 4016 (beside the bright yellow star). Clump 19 is North of the top of this figure so is not seen.

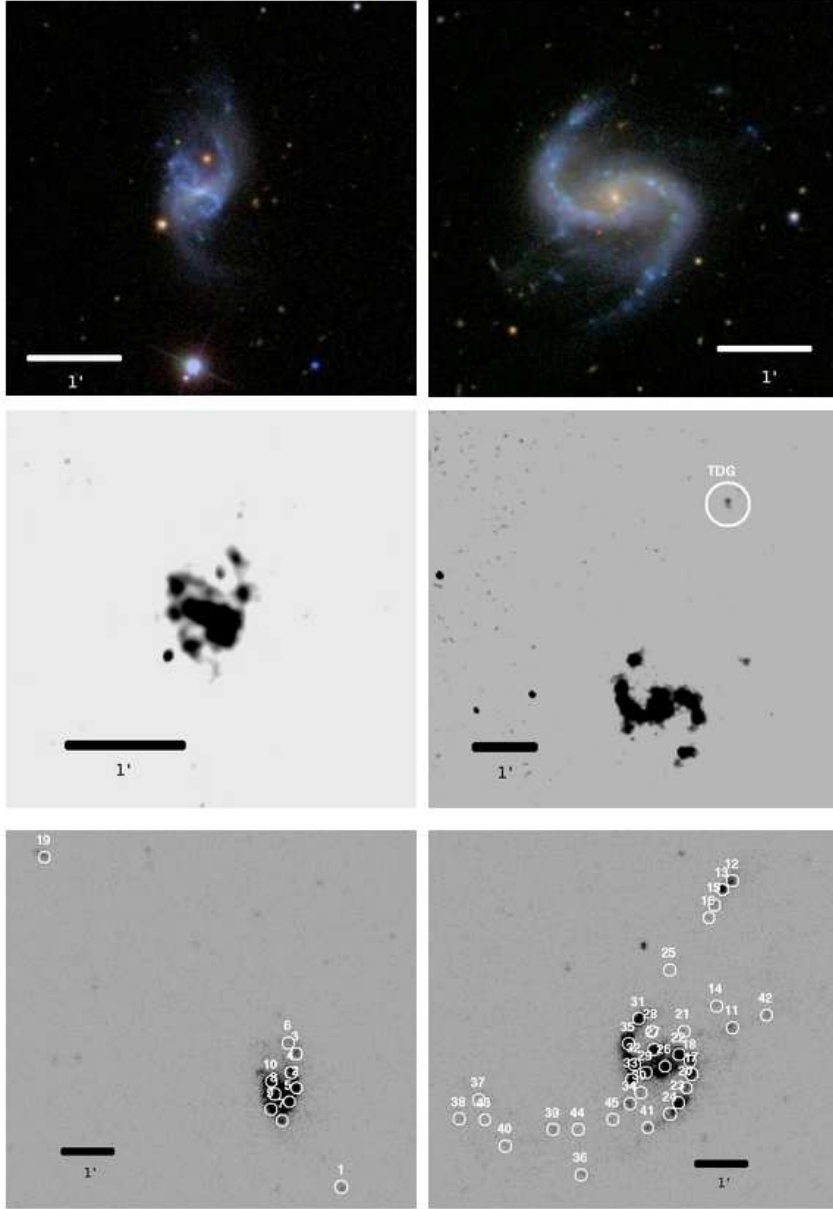


Fig. 2.— Top Left: Composite *ugriz* SDSS image of NGC 4016. North is up and East is to the left. Notice the striking figure eight shaped feature. Clump 1 is seen clearly southwest of the galaxy (beside the bright star). Top Right: Composite *ugriz* SDSS image of NGC 4017. Middle Left: Smoothed continuum-subtracted  $H\alpha$  image of NGC 4016 obtained with SARA. The tidal arms and the Northern part of the figure eight features are seen. Middle Right: Smoothed continuum-subtracted  $H\alpha$  image of NGC 4017 obtained with SARA. The bridge TDG is clearly detected at the top of this figure. Bottom Left: FUV GALEX image of the Northern galaxy NGC 4016 with clumps labeled. Notice the TDG candidates, one to the South (clump 1) and one to the North (clump 19). The circles around each clump have radii of  $5''$  and are the same size as those used for the photometry. Bottom Right: FUV GALEX image of the southern galaxy NGC 4017 with clumps labeled. Notice the TDG candidate to the North (Bridge TDG, clumps 12, 13, 15, and 16). In each panel North is up and East is to the left.

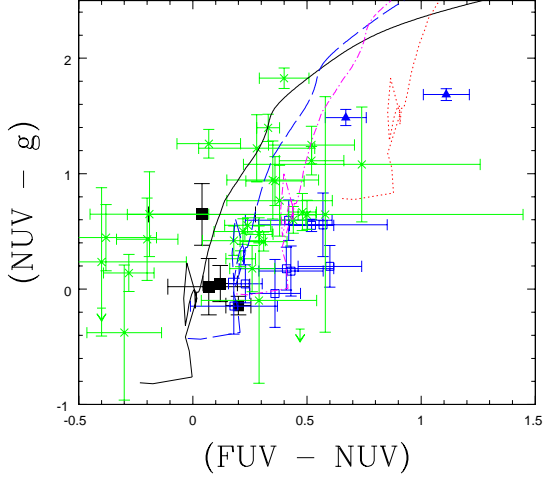


Fig. 3.— FUV-NUV vs NUV-g color-color plot. The solid black squares are clumps in the bridge TDG (clumps 12, 13, 15, and 16), the open blue squares are clumps in NGC 4016, the solid blue triangles are clump 1 and clump 19, and a green x represents clumps in NGC 4017. The curves are SB99 models with  $E(B-V)$  of 0 (solid black), 0.12 (long dashed blue), 0.25 (dot dashed magenta), and 0.5 (dotted red).

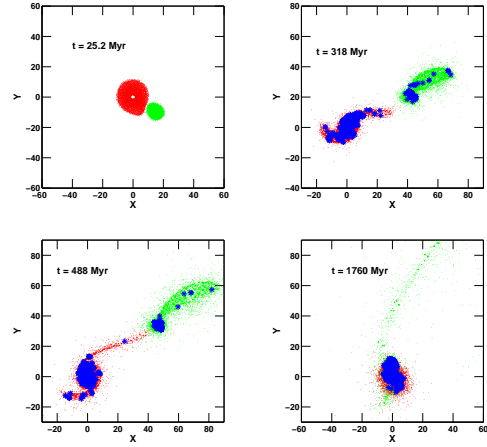


Fig. 4.— Snapshots of the model gas disks from a time near closest passage to merger. The current appearance of Arp 305 best matches the views shown in the top right and the lower left panels, i.e.,  $\sim 300 - 400$  Myr after closest approach. Red particles originated in the primary galaxy, green in the companion. The top left panel shows a time near closest approach. Every fifth particle from the simulation is plotted. The axis are in kpc in the adopted scaling. In the last three panels blue asterisks mark star-forming particles. The companion forms stars actively at most times after closest approach. Star formation is common in tidal structures at intermediate times.

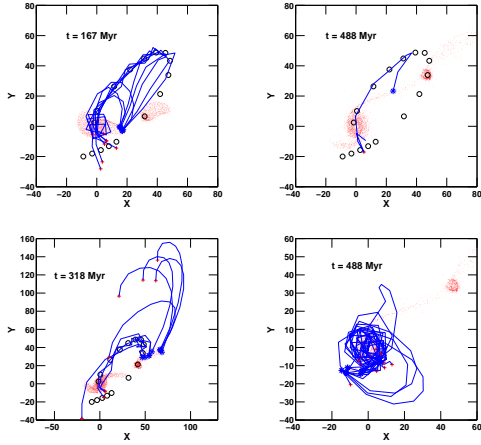


Fig. 5.— Illustrations of the orbital trajectories of star-forming particles from the onset of star formation in the bridge to the end of the run when the galaxies have merged, overplotted on the gas particle distributions at selected times in the interaction. Red dots show the locations of gas particles, at the time of SF onset in the selected particles. Black circles show the position of the companion center at selected time-steps from closest passage to merger. Blue asterisks show star-forming particles in selected tidal structures. The timestep of the panel is chosen as the time when these selected particles have just recently turned on star formation, so we can follow the subsequent orbit of these ‘star clusters’. The axis are in kpc in the adopted scaling. Blue curves connecting each asterisk to a red plus sign show the particle trajectory from the onset of SF to the end of the run when the two galaxies have merged. Note that the particles continue to be gas particles, subject to hydrodynamical forces, in contrast to the star cluster that would have formed within the particle. Nonetheless, it appears that the role of hydrodynamic forces is small until such time as the particle collides with a galaxy disk. Note also that while the companion galaxy is subject to dynamical friction (leading to merger), the individual particles are not. Given the small mass of the particles, frictional effects should not be large, except for those passing close to the center of a galaxy. Note: because of the large excursions of the countertail particles, the scale of the lower left panel is larger than that of the other panels.

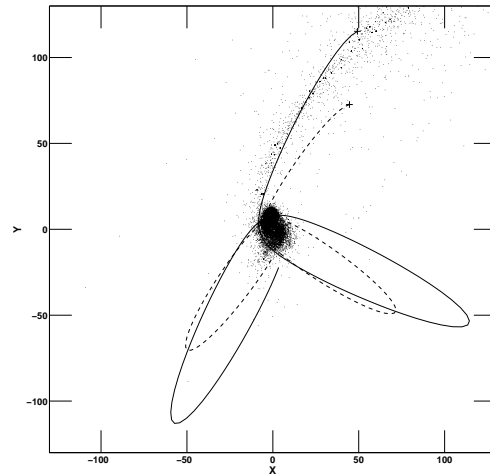


Fig. 6.— Analytic extension of the orbits of two candidate tidal dwarf galaxies (solid and dashed curves), calculated as described in the text. The dots show the gas distribution at the end of the numerical simulation, as in the last panel of Figure 4. Crosses mark the start of the extended trajectories, see text for more details. The axis are in kpc in the adopted scaling.



Table 1: Global Magnitudes

ID	FUV mag	NUV mag	u mag	g mag	r mag	i mag	z mag
Bridge TDG	17.90±0.019	17.86±0.016	≥19.16	17.83±0.122	17.59±0.175	17.73±0.385	17.71±1.516
NGC 4016	15.41±0.006	14.87±0.003	14.97±0.051	14.00±0.007	13.64±0.009	13.43±0.013	13.31±0.056
NGC 4017	14.93±0.005	14.44±0.003	14.07±0.036	13.01±0.004	12.50±0.005	12.25±0.008	12.21±0.030

Table 2: Bridge TDG Clump Magnitudes

Clump	ID	FUV mag	NUV mag	u mag	g mag	r mag	i mag	z mag
12	Bridge TDG	20.0±0.06	19.9±0.04	20.6±0.36	19.9±0.14	19.9±0.13	20.1±0.22	≥19.5
13	Bridge TDG	19.5±0.05	19.3±0.02	19.5±0.14	19.4±0.07	19.5±0.10	19.6±0.21	≥19.5
15	Bridge TDG	21.3±0.10	21.2±0.14	≥21.3	21.2±0.19	21.1±0.28	20.8±0.42	≥19.5
16	Bridge TDG	21.8±0.12	21.8±0.20	≥21.3	21.1±0.17	20.9±0.44	20.5±0.42	≥19.5

Table 3: NGC 4016 Clump Magnitudes

Clump	ID	FUV mag	NUV mag	u mag	g mag	r mag	i mag	z mag
1	n4016 tidal	21.2±0.09	20.1±0.04	19.6±0.16	18.4±0.02	18.6±0.04	18.8±0.10	19.0±0.48
2	n4016 disk	19.2±0.12	18.8±0.14	19.0±0.36	18.2±0.10	18.0±0.10	18.0±0.14	18.5±0.30
3	n4016 disk	20.8±0.09	20.2±0.09	20.2±0.20	20.0±0.15	19.8±0.11	20.2±0.22	≥19.5
4	n4016 disk	19.7±0.11	19.3±0.08	19.9±0.26	19.1±0.19	19.1±0.21	19.9±0.24	≥19.5
5	n4016 disk	18.1±0.13	17.7±0.16	17.9±0.15	17.5±0.09	17.2±0.07	17.2±0.13	17.5±0.42
6	n4016 disk	21.1±0.17	20.9±0.08	≥21.3	21.1±0.22	21.0±0.28	≥21.2	≥19.5
7	n4016 disk	19.8±0.10	19.5±0.04	20.1±0.41	19.5±0.29	19.5±0.33	20.5±0.86	≥19.5
8	n4016 disk	18.3±0.09	17.8±0.02	17.8±0.10	17.3±0.04	16.9±0.06	16.8±0.14	17.0±0.25
9	n4016 disk	19.2±0.17	18.6±0.22	19.1±0.45	18.1±0.16	17.9±0.19	18.0±0.22	19.2±0.83
10	n4016 disk	18.4±0.05	18.1±0.05	18.6±0.15	18.1±0.15	18.1±0.23	18.2±0.26	18.9±0.34
19	n4016 tidal	20.9±0.08	20.3±0.04	19.8±0.26	18.8±0.05	18.3±0.04	18.1±0.13	18.0±0.22

<sup>a</sup> Note: the nucleus is between clumps 5 and 8 (see Figure 5)

Table 4: NGC 4017 Clump Magnitudes

Clump	ID	FUV mag	NUV mag	u mag	g mag	r mag	i mag	z mag
11	n4017 tidal	20.7±0.08	20.4±0.05	20.7±0.33	20.0±0.06	20.0±0.11	≥21.2	19.5±0.57
14	n4017 tidal	21.3±0.09	21.2±0.10	≥21.3	20.0±0.06	19.4±0.07	19.3±0.10	19.5±0.53
17	n4017 disk	19.6±0.09	19.4±0.08	19.0±0.08	18.9±0.07	18.3±0.17	18.6±0.19	18.2±0.23
18	n4017 disk	19.4±0.08	18.9±0.11	18.4±0.07	17.8±0.05	17.5±0.07	17.3±0.05	17.3±0.09
20	n4017 tidal	20.5±0.16	20.2±0.19	19.9±0.18	19.0±0.21	18.9±0.15	19.0±0.13	18.8±0.26
21	n4017 tidal	21.9±0.31	22.3±0.19	≥21.3	22.0±0.61	≥21.8	≥21.2	≥19.5
22	n4017 hinge	18.5±0.03	18.0±0.02	17.6±0.04	17.4±0.12	17.1±0.15	17.1±0.15	16.9±0.09
23	n4017 tidal	18.8±0.03	18.6±0.05	18.6±0.07	18.3±0.04	18.2±0.11	18.5±0.07	18.9±0.42
24	n4017 tidal	20.1±0.08	19.8±0.05	20.4±0.26	19.7±0.19	19.7±0.25	19.5±0.23	≥19.5
25	n4017 tidal	22.3±0.15	22.5±0.21	≥21.3	21.8±0.29	20.6±0.20	20.0±0.20	≥19.5
26	n4017 nucleus	18.8±0.04	18.5±0.02	18.0±0.06	17.1±0.11	16.3±0.19	16.0±0.15	15.9±0.15
27	n4017 disk	19.2±0.17	18.8±0.15	19.0±0.43	18.1±0.26	17.6±0.27	17.5±0.28	18.1±0.92
28	n4017 tidal	23.0±0.57	22.5±0.64	≥21.3	21.8±0.79	21.8±1.15	≥21.2	≥19.5
29	n4017 disk	18.9±0.12	18.6±0.02	18.0±0.10	17.6±0.21	17.6±0.38	17.8±0.50	17.3±0.15
30	n4017 disk	22.3±0.36	21.5±0.36	21.2±0.50	20.5±0.33	20.2±0.37	20.2±0.32	≥19.5
31	n4017 tidal	18.8±0.04	18.5±0.04	18.4±0.07	18.0±0.05	17.9±0.05	18.0±0.07	18.1±0.14
32	n4017 hinge	18.3±0.08	18.1±0.05	18.0±0.08	17.5±0.03	17.2±0.07	17.2±0.15	17.3±0.12
33	n4017 disk	19.2±0.04	18.7±0.03	18.8±0.20	18.1±0.10	17.9±0.10	17.9±0.10	19.3±0.72
34	n4017 tidal	20.5±0.08	20.4±0.11	20.7±0.43	19.9±0.06	19.7±0.08	19.6±0.15	19.5±0.48
35	n4017 tidal	18.9±0.04	18.4±0.04	18.4±0.14	17.7±0.15	17.5±0.06	17.6±0.17	17.6±0.12
36	n4017 tidal	21.3±0.09	20.9±0.06	20.2±0.19	19.0±0.06	18.5±0.05	18.3±0.05	18.2±0.14
37	n4017 tidal	22.1±0.17	21.9±0.17	≥21.3	21.9±0.69	≥21.8	≥21.2	≥19.5
38	n4017 tidal	21.6±0.11	21.9±0.12	≥21.3	22.3±0.57	21.5±0.77	≥21.2	19.3±0.42
39	n4017 tidal	21.4±0.1	21.7±0.19	≥21.3	21.3±0.20	21.2±0.30	21.0±0.69	≥19.5
40	n4017 tidal	21.9±0.12	22.3±0.15	≥21.3	≥22.5	≥21.8	≥21.2	≥19.5
41	n4017 tidal	20.7±0.08	21.±0.07	20.8±0.58	20.8±0.14	20.8±0.22	21.0±0.58	≥19.5
42	n4017 tidal	21.2±0.09	21.4±0.1	21.1±0.49	20.9±0.34	≥21.8	21.2±999.	≥19.5
43	n4017 tidal	22.0±0.13	21.5±0.13	≥21.3	20.3±0.08	20.1±0.11	18.4±2.79	≥19.5
44	n4017 tidal	22.4±0.15	22.0±0.13	≥21.3	21.1±0.31	20.1±0.11	21.2±999.	19.5±0.72
45	n4017 tidal	22.6±0.32	22.1±0.19	≥21.3	≥22.5	21.2±0.47	19.6±0.33	≥19.5

Table 5: Age and E(B–V) Estimates

Clump	ID	R.A. (deg)	DEC (deg)	Ages (Myr)	E(B–V) (mag)	Colors Used <sup>a</sup>
1	n4016 tidal	179.60528	27.508193	236 <sup>+23</sup> <sub>-26</sub>	0.00 <sup>+0.04</sup> <sub>-0.00</sub>	FUV–NUV, NUV–g, u–g, g–r, r–i, i–z
2	n4016 disk	179.61702	27.531111	6 <sup>+85</sup> <sub>-1</sub>	0.22 <sup>+0.12</sup> <sub>-0.22</sub>	FUV–NUV, NUV–g, u–g, g–r, r–i, i–z
3	n4016 disk	179.61702	27.539028	4 <sup>+3</sup> <sub>-1</sub>	0.26 <sup>+0.12</sup> <sub>-0.18</sub>	FUV–NUV, NUV–g, u–g, g–r, r–i
4	n4016 disk	179.61843	27.534653	5 <sup>+2</sup> <sub>-2</sub>	0.22 <sup>+0.14</sup> <sub>-0.16</sub>	FUV–NUV, NUV–g, u–g, g–r, r–i
5	n4016 disk	179.6189	27.527778	8 <sup>+24</sup> <sub>-3</sub>	0.10 <sup>+0.16</sup> <sub>-0.10</sub>	FUV–NUV, NUV–g, u–g, g–r, r–i, i–z
6	n4016 disk	179.61914	27.541528	4 <sup>+27</sup> <sub>-1</sub>	0.12 <sup>+0.12</sup> <sub>-0.12</sub>	FUV–NUV, NUV–g, g–r
7	n4016 disk	179.62071	27.523611	4 <sup>+29</sup> <sub>-2</sub>	0.20 <sup>+0.14</sup> <sub>-0.18</sub>	FUV–NUV, NUV–g, u–g, g–r, r–i
8	n4016 disk	179.62266	27.529653	11 <sup>+16</sup> <sub>-6</sub>	0.22 <sup>+0.06</sup> <sub>-0.10</sub>	FUV–NUV, NUV–g, u–g, g–r, r–i, i–z
9	n4016 disk	179.6236	27.526111	6 <sup>+134</sup> <sub>-3</sub>	0.24 <sup>+0.22</sup> <sub>-0.24</sub>	FUV–NUV, NUV–g, u–g, g–r, r–i, i–z
10	n4016 disk	179.6236	27.532569	6 <sup>+30</sup> <sub>-3</sub>	0.10 <sup>+0.14</sup> <sub>-0.10</sub>	FUV–NUV, NUV–g, u–g, g–r, r–i, i–z
11	n4017 tidal	179.67126	27.460685	6 <sup>+39</sup> <sub>-1</sub>	0.16 <sup>+0.06</sup> <sub>-0.16</sub>	FUV–NUV, NUV–g, u–g, g–r
12	Bridge TDG	179.67128	27.494644	6 <sup>+32</sup> <sub>-2</sub>	0.06 <sup>+0.10</sup> <sub>-0.06</sub>	FUV–NUV, NUV–g, u–g, g–r, r–i
13	Bridge TDG	179.67386	27.492559	15 <sup>+6</sup> <sub>-11</sub>	0.04 <sup>+0.10</sup> <sub>-0.04</sub>	FUV–NUV, NUV–g, u–g, g–r, r–i
14	n4017 tidal	179.67549	27.465684	8 <sup>+35</sup> <sub>-2</sub>	0.34 <sup>+0.08</sup> <sub>-0.14</sub>	FUV–NUV, NUV–g, g–r, r–i, i–z
15	Bridge TDG	179.67597	27.489017	15 <sup>+27</sup> <sub>-11</sub>	0.06 <sup>+0.16</sup> <sub>-0.06</sub>	FUV–NUV, NUV–g, g–r, r–i
16	Bridge TDG	179.67738	27.4861	39 <sup>+77</sup> <sub>-34</sub>	0.04 <sup>+0.30</sup> <sub>-0.04</sub>	FUV–NUV, NUV–g, g–r, r–i
17	n4017 disk	179.68182	27.449848	5 <sup>+7</sup> <sub>-2</sub>	0.26 <sup>+0.10</sup> <sub>-0.12</sub>	FUV–NUV, NUV–g, u–g, g–r, r–i, i–z
18	n4017 disk	179.68229	27.452973	6 <sup>+77</sup> <sub>-1</sub>	0.38 <sup>+0.08</sup> <sub>-0.30</sub>	FUV–NUV, NUV–g, u–g, g–r, r–i, i–z
19	n4016 tidal	179.68283	27.584431	7 <sup>+43</sup> <sub>-2</sub>	0.40 <sup>+0.10</sup> <sub>-0.14</sub>	FUV–NUV, NUV–g, u–g, g–r, r–i, i–z
20	n4017 tidal	179.68323	27.446722	140 <sup>+124</sup> <sub>-135</sub>	0.00 <sup>+0.44</sup> <sub>-0.00</sub>	FUV–NUV, NUV–g, u–g, g–r, r–i, i–z
21	n4017 tidal	179.68394	27.459847	7 <sup>+62</sup> <sub>-6</sub>	0.00 <sup>+0.30</sup> <sub>-0.00</sub>	FUV–NUV, NUV–g
22	n4017 hinge	179.68511	27.45443	6 <sup>+19</sup> <sub>-2</sub>	0.26 <sup>+0.08</sup> <sub>-0.06</sub>	FUV–NUV, NUV–g, u–g, g–r, r–i, i–z
23	n4017 tidal	179.68534	27.443388	6 <sup>+1</sup> <sub>-1</sub>	0.12 <sup>+0.04</sup> <sub>-0.06</sub>	FUV–NUV, NUV–g, u–g, g–r, r–i, i–z
24	n4017 tidal	179.68745	27.440679	12 <sup>+38</sup> <sub>-8</sub>	0.12 <sup>+0.14</sup> <sub>-0.12</sub>	FUV–NUV, NUV–g, u–g, g–r, r–i
25	n4017 tidal	179.6877	27.474012	9 <sup>+24</sup> <sub>-2</sub>	0.22 <sup>+0.20</sup> <sub>-0.22</sub>	FUV–NUV, NUV–g, g–r, r–i
26	n4017 nucleus	179.68886	27.45172	130 <sup>+84</sup> <sub>-87</sub>	0.04 <sup>+0.18</sup> <sub>-0.04</sub>	FUV–NUV, NUV–g, u–g, g–r, r–i, i–z
27	n4017 disk	179.69168	27.455677	8 <sup>+178</sup> <sub>-5</sub>	0.26 <sup>+0.24</sup> <sub>-0.26</sub>	FUV–NUV, NUV–g, u–g, g–r, r–i, i–z
28	n4017 tidal	179.69239	27.459843	6 <sup>+382</sup> <sub>-5</sub>	0.24 <sup>+0.60</sup> <sub>-0.24</sub>	FUV–NUV, NUV–g, g–r
29	n4017 disk	179.69379	27.450259	34 <sup>+119</sup> <sub>-30</sub>	0.16 <sup>+0.24</sup> <sub>-0.16</sub>	FUV–NUV, NUV–g, u–g, g–r, r–i, i–z
30	n4017 disk	179.6952	27.445675	6 <sup>+321</sup> <sub>-3</sub>	0.38 <sup>+0.36</sup> <sub>-0.38</sub>	FUV–NUV, NUV–g, u–g, g–r, r–i
31	n4017 tidal	179.69568	27.462758	6 <sup>+1</sup> <sub>-1</sub>	0.16 <sup>+0.06</sup> <sub>-0.04</sub>	FUV–NUV, NUV–g, u–g, g–r, r–i, i–z
32	n4017 hinge	179.69685	27.452132	8 <sup>+5</sup> <sub>-3</sub>	0.18 <sup>+0.06</sup> <sub>-0.06</sub>	FUV–NUV, NUV–g, u–g, g–r, r–i, i–z
33	n4017 disk	179.69755	27.44859	6 <sup>+27</sup> <sub>-1</sub>	0.24 <sup>+0.06</sup> <sub>-0.10</sub>	FUV–NUV, NUV–g, u–g, g–r, r–i, i–z
34	n4017 tidal	179.69801	27.443173	12 <sup>+31</sup> <sub>-7</sub>	0.14 <sup>+0.10</sup> <sub>-0.14</sub>	FUV–NUV, NUV–g, u–g, g–r, r–i, i–z
35	n4017 tidal	179.69826	27.456923	6 <sup>+25</sup> <sub>-2</sub>	0.26 <sup>+0.10</sup> <sub>-0.08</sub>	FUV–NUV, NUV–g, u–g, g–r, r–i, i–z
36	n4017 tidal	179.71068	27.426708	70 <sup>+76</sup> <sub>-64</sub>	0.30 <sup>+0.22</sup> <sub>-0.16</sub>	FUV–NUV, NUV–g, u–g, g–r, r–i, i–z
37	n4017 tidal	179.73745	27.44398	4 <sup>+80</sup> <sub>-3</sub>	0.16 <sup>+0.30</sup> <sub>-0.16</sub>	FUV–NUV, NUV–g
38	n4017 tidal	179.74238	27.4396	1 <sup>+12</sup> <sub>-0</sub>	0.00 <sup>+0.16</sup> <sub>-0.00</sub>	FUV–NUV, NUV–g, g–r
39	n4017 tidal	179.71796	27.437119	7 <sup>+60</sup> <sub>-2</sub>	0.00 <sup>+0.16</sup> <sub>-0.00</sub>	FUV–NUV, NUV–g, g–r, r–i
40	n4017 tidal	179.7304	27.43336	1 <sup>+2</sup> <sub>-0</sub>	0.00 <sup>+0.06</sup> <sub>-0.00</sub>	FUV–NUV
41	n4017 tidal	179.69331	27.437551	7 <sup>+27</sup> <sub>-2</sub>	0.00 <sup>+0.08</sup> <sub>-0.00</sub>	FUV–NUV, NUV–g, u–g, g–r, r–i
42	n4017 tidal	179.66234	27.463605	7 <sup>+30</sup> <sub>-1</sub>	0.00 <sup>+0.06</sup> <sub>-0.00</sub>	FUV–NUV, NUV–g
43	n4017 tidal	179.7358	27.439398	43 <sup>+133</sup> <sub>-38</sub>	0.22 <sup>+0.22</sup> <sub>-0.22</sub>	FUV–NUV, NUV–g, g–r, r–i
44	n4017 tidal	179.71139	27.437124	8 <sup>+28</sup> <sub>-7</sub>	0.30 <sup>+0.20</sup> <sub>-0.16</sub>	FUV–NUV, NUV–g, g–r
45	n4017 tidal	179.70247	27.439421	9 <sup>+121</sup> <sub>-2</sub>	0.38 <sup>+0.32</sup> <sub>-0.32</sub>	FUV–NUV, r–i

<sup>a</sup> We did not include upper limits in our fits